ELSEVIER

International Journal of Mass Spectrometry 202 (2000) 147–160

International Journal of Mass Spectrometry

On mass discrimination in high-pressure mass spectrometry: potential errors in measurements leading to absolute ion abundances

Jamey K. Hovey*, Alexander Likholyot

Mass Spectrometry Laboratory, Geochemistry Group, Institute of Mineralogy and Petrography, ETH-Zentrum (Swiss Federal Institute of Technology), Sonneggstrasse 5, CH-8092, Zurich, Switzerland

Received 15 November 1999; accepted 20 March 2000

Abstract

Various thermochemical calculations require that mass spectrometric measurements provide absolute values for ratios of ion abundances. High-pressure mass spectrometric measurements normally employ a small slit between a high-pressure reaction chamber and the ion detection vacuum envelope. It is shown that the sampling of ions through a small slit depends classically on the square root of mass when flow through the slit can be characterized as molecular. Calculations that require ion intensity or abundance ratios, such as equilibrium constants or standard Gibbs energies of reaction, need to consider this mass effect. The nature of mass discrimination in high-pressure and stationary afterglow experiments has been characterized for traditional ion sampling through a thin slit and also for the various ion-diffusion processes present in these experiments. It has been shown that thermodynamic values obtained considering this effect are in better agreement with other measurements free of mass discrimination. (Int J Mass Spectrom 202 (2000) 147–160) © 2000 Elsevier Science B.V.

Keywords: High pressure mass spectrometry; Mass discrimination; Ion sampling; Stationary afterglow

1. Introduction

Measurements leading to the thermodynamic properties of gas-phase ions are extremely important tools for the investigation of a variety of processes including ionic solvation, organic reaction mechanisms, and interstellar processes to name a few [1]. Techniques that can lead to well-defined quantum and thermodynamic states are particularly useful in this regard. Pulsed-electron high pressure mass spectrometry is one such technique whereby experimental conditions are well-favoured for thermodynamic measurements of a well-defined thermodynamic state for the system under investigation.

Although several techniques can be used to determine gas-phase reaction energy profiles, only a few techniques [for example high-pressure mass spectrometry (HPMS) and ion-cyclotron resonance (ICR) mass spectrometry] lead directly to equilibrium distributions and hence the change in Gibbs free energy for these reactions. For experiments investigated by HPMS, it is believed that because of the high number density of neutral gas particles, a meaningful thermodynamic state, temperature, pressure, and thus reaction profile are defined. For both of these techniques,

* Corresponding author. E-mail: hovey@erdw.ethz.ch

PII S1387-3806(00)00234-7

the change in standard state Gibbs energy ΔG° can be written

$$\Delta G^\circ = -RT \ln K_{eq} \quad (1)$$

where K_{eq} is the equilibrium constant for the reaction under investigation. A typical reaction (in this case for proton transfer) can be written

$$B_1H^+ + B_2 = B_2H^+ + B_1 \quad (2)$$

where neutral species are designated as B_n. The thermodynamic equilibrium constant is written in terms of the activities of each participating species:

$$K_{eq} = \frac{a_{B_2H^+} \cdot a_{B_1}}{a_{B_1H^+} \cdot a_{B_2}} \quad (3)$$

In terms of gas-phase experiments at relatively low pressure, we can assume that the gases and ions behave as perfect gases. As such, after sufficient reaction time the thermodynamic equilibrium constant may be represented by:

$$K_{eq} = \frac{I_{B_2H^+} \cdot p_{B_1}}{I_{B_1H^+} \cdot p_{B_2}} \quad (4)$$

where I represents ion abundances as measured experimentally, and p represents partial pressures of neutral species, where both quantities are used to approximate number densities or absolute concentrations. K_{eq} is a function only of temperature when the various concentrations are represented by partial pressures (perfect gases) and as such it is assumed that the ratio of ionic abundances equals the ratio of partial pressures of the ions.

The enthalpy of a reaction is related by the temperature dependence of the equilibrium constant:

$$\left(\frac{\partial \ln K_{eq}}{\partial T}\right)_p = \frac{\Delta H^\circ}{RT^2} \quad (5)$$

Variation of temperature in certain mass spectrometric experiments allows calculation of ΔH° and subsequently ΔS° via

$$\left(\frac{\partial \Delta G^\circ}{\partial T}\right)_p = -\Delta S^\circ \quad (6)$$

HPMS experiments normally use this derivative technique to determine the associated enthalpies for reactions of type given by Eq. 2, whereas ICR experiments normally rely on an extrathermodynamic assumption of the entropy change to allow calculation of the change in enthalpy.

A high ion source pressure in the HPMS experiment favours equilibrium (when appropriate for a given set of reaction conditions) as opposed to long ion-trapping times favouring reaction and equilibrium during the ICR experiment. Whereas ICR allows all ions to be sampled with near identical efficiency [2], because of its *in situ* nature, in HPMS and other forms of mass spectrometry, ions are sampled through a small orifice or slit [3], and are often subject to external or internal (space-charge) fields that may alter the "detection efficiency" of the sample. It is in these cases where potential problems associated with mass discrimination occur.

Most techniques involving mass spectrometry (especially those employing quadrupole mass filters) have considered mass discrimination during ion sampling. However, even though implied in early discussions, it appears that a quantitative discussion of ionic mass discrimination during sampling (prior to the mass discrimination inherent in detection systems) in HPMS and other related techniques, has largely been ignored. Grimsrud and co-workers [4–6], however, have considered the ion sampling process in HPMS in some detail. They have identified several sources of errors including the discrimination due to the preferential depletion of lighter mass neutral molecules in the HPMS experiment [4,5].

2. Theory

2.1. Brief background

Various authors have presented accounts of the HPMS experiment but none as complete as the main developer—Kebarle [3]. It is important here to consider the nature of the HPMS experiment including the *average* dimensions and conditions existing inside a typical reaction chamber.

An HPMS experiment consists of a short electron pulse acting on a mixture of a small amount of reactant in a large excess of bath gas. The bath gas is present in the HPMS experiment as a thermalizer (ions and electrons), and often to aid in the ionization process and as a source for third body collisions. Following a short electron pulse, the conditions inside the HPMS source can be described as an electrical plasma containing electrons, positive ions, and negative ions. A detailed description of this condition has been presented by Kebarle [3] and Hiraoka [7]. There is a wealth of information [8] that has been published regarding mobilities of ions and electrons in neutral gases that can be used to directly determine the conditions and potential mass discrimination of HPMS and stationary afterglow experiments (of which HPMS is an example).

A discussion of mass discrimination must first begin by consideration of the energy or velocity distribution of ions and gases. More than 100 years ago Graham [9] noted that the escape of gases through small orifices was a function of the gas density (hence pressure) and the square root of the mass of the gas. Graham's law can be expressed:

$$\frac{f_1}{f_2} = \left(\frac{M_2}{M_1}\right)^{1/2} \tag{7}$$

where f is the flux of gas leaving the orifice and M_i is the respective molecular weight of the gas.

A convenient starting point in the discussion of gaseous physical properties rests in the kinetic theory of gases [10]. In the absence of any external fields, the Maxwellian velocity distribution can be written:

$$\frac{dn}{dv} = \frac{2N}{\sqrt{\pi}}\left(\frac{m}{2kT}\right)^{3/2} v^2 \exp\left(\frac{-mv^2}{2kT}\right) \tag{8}$$

that results in an average particle velocity $\bar{v}$:

$$\bar{v} = \left(\frac{8kT}{\pi m}\right)^{1/2} \tag{9}$$

where n is the number of particles with mass m, v is the velocity, N is the total number of particles, k is Boltzmann's constant, and T is the absolute temperature. Eq. (9) is an important result because it immediately shows the dependence of the gas velocity on the square root of mass that appears in a variety of gaseous flow equations.

2.2. Stationary afterglow

Although most stationary afterglow experiments have been replaced by the more versatile flowing afterglow experiments, there are a variety of results pertaining to static afterglow experiments of which HPMS can be considered. The characterization of an afterglow as having a substantial number of ionized particles following initial ionization is true in the HPMS experiment.

We begin by considering Fick's law of diffusion even though it is inherently based on a system of identical particles interacting only through short-lived two-body collisions [11]. Because the concentration of ions is normally significantly less than the neutral bath gas, the individual ions can be considered to be interacting only with neutral gas and as such Fick's law should apply. Fick's law can be written for the diffusion of a gas in the absence of any externally applied fields and shall be denoted as free diffusion:

$$\Gamma_i = -D_i \nabla n_i \tag{10}$$

where Γ_i is the diffusion current density that is proportional to the free diffusion coefficient D_i multiplied by the gradient and concentration of ions n_i. In the presence of an electric field Γ_i becomes the sum of free diffusion (driven by a concentration gradient) and field-induced diffusion (driven by a permanent or induced electric field) for particles of type i by:

$$\Gamma_i = -D_i \nabla n_i + n_i \mu_i E \tag{11}$$

where $D_i \nabla n_i$ is the contribution to diffusion due to the concentration gradient, $n_i \mu_i E$ is the contribution due to field-induced mobility of the particle, and μ_i is the corresponding ionic mobility.

In a stationary afterglow or HPMS experiment characterized by an ionization pulse for sufficient ion density, the electrical plasma thereby created is characterized initially by ambipolar diffusion of positive ions and electrons. In the special case of only one

positive ion, or of several positive ions with the same ionic mobility, the fluxes can be written:

$$\Gamma^+ = -D^+\nabla n^+ + n^+\mu^+ E \tag{12}$$

$$\Gamma_e = -D_e\nabla n_e - n_e\mu_e E \tag{13}$$

and after appropriate algebraic rearrangement considering that fluxes of positive ions and electrons are approximately equal [11], and elimination of the electric field E leads to the standard ambipolar diffusion equation:

$$\Gamma = -D_a\nabla n \tag{14}$$

where

$$D_a = \frac{D^+\mu_e + D_e\mu^+}{\mu_e + \mu^+} \tag{15}$$

The ionic mobilities can be substituted into this ambipolar diffusion equation (for a Maxwellian distribution and equal electron and ion temperatures):

$$D = \frac{\mu kT}{e} \tag{16}$$

and therefore

$$\frac{D^+}{\mu^+} = \frac{D_e}{\mu_e} = \frac{kT}{e} \tag{17}$$

then

$$D_a = \frac{2D^+\mu_e}{\mu_e + \mu^+} \approx 2D^+ \tag{18}$$

and D_a is approximately equal to $2D^+$ because of the very large difference between electron and ion mobilities: $\mu_e \gg \mu^+$. Ambipolar electron-ion diffusion is, however, only valid whilst an electrical plasma is maintained (the case where $|n^+ - n_e| \ll n_e$).

In an experiment with several long-lived ions (as is normally the case for HPMS experiments) and electrons, and for the case of two positive ions (denoted by subscripts 1 and 2), we can write:

$$\Gamma_1^+ = -D_1^+\nabla n_1^+ + n_1^+\mu_1^+ E \tag{19}$$

$$\Gamma_2^+ = -D_2^+\nabla n_2^+ + n_2^+\mu_2^+ E \tag{20}$$

$$\Gamma_e = -D_e\nabla n_e - n_e\mu_e E \tag{21}$$

at sufficiently high electron densities, the ion fluxes are controlled by the ambipolar diffusion coefficients as discussed above. In a similar fashion, the electron density can be related to an effective diffusion coefficient D^* by:

$$\Gamma_e = -D^*\nabla n_1 \tag{22}$$

where

$$D^* = \frac{D_e(\mu_1 + K\mu_2) + \mu_e(D_1^+ + KD_2^+)}{\mu_1 + K\mu_2 + \mu_e} \tag{23}$$

which is exactly analogous to a weighted ambipolar diffusion coefficient given by Eq. (15) if the two positive ion concentrations can be related arbitrarily by $K = n_1/n_2$ (as can be assumed at some point in an equilibrium reaction) and that if only two cations are present,

$$\Gamma_e = \Gamma_1^+ + \Gamma_2^+ \tag{24}$$

noting that D^* reduces to D_a when $n_2 = n_1$.

At sufficiently long times following the finite ionization pulse or event, the diffusion of ionic species changes from cation–electron ambipolar to cation–anion ambipolar diffusion [12] or to free diffusion if the concentration of ionic species are too low. It is of primary importance here to consider the flux of ions reaching the wall as a function of experimental conditions. Following Massey [13], a simple afterglow experiment can be characterized by the time-dependent concentrations of the species. Assuming that HPMS will ordinarily have a minimum of two positive ions (concentrations designated by n_1 and n_2), some number of metastable species n_m in early stages, and some number of negative ions (n_-) in later stages, we can derive region specific formulae.

2.3. Region I: Ionization and cation–electron ambipolar diffusion

A simple plot defining each of the three main regions in a typical HPMS (at high ionization) or stationary afterglow is given in Fig. 1. Region I is

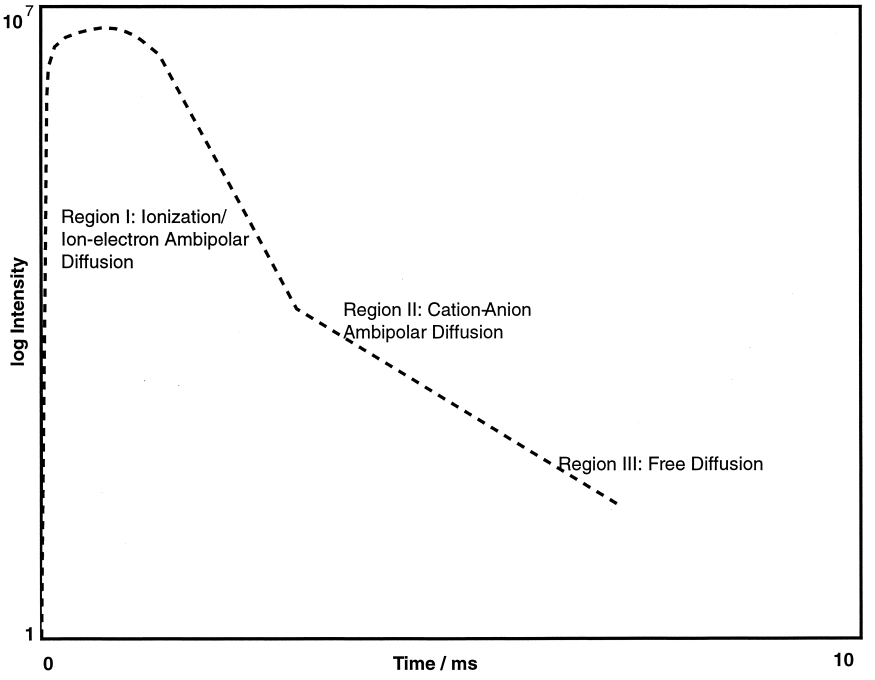

Fig. 1. Qualitative display of regions for various modes of diffusion in a typical HPMS experiment with initially high ionization density (at $t = 0$).

characterized by initial ionization and decay of metastable species leading to cation–electron ambipolar diffusion. It is sufficient here to start with two ionic species present initially and not reacting with each other to any great extent. Time dependent diffusion equations can be written for the two ionic species in the absence of sources or sinks for these species:

$$\frac{\partial n_1(r, t)}{\partial t} = -D_{1a}\nabla^2 n_1(r, t) \tag{25}$$

$$\frac{\partial n_2(r, t)}{\partial t} = -D_{2a}\nabla^2 n_2(r, t) \tag{26}$$

negative ion diffusion to the walls is hindered because of the self-field created by positive ions and electrons, and ionic distributions here are assumed free of metastables. These equations can be solved easily for the case of a spherical geometry (for example in our mass spectrometer we have a slightly complicated cylindrical shape that is easily approximated to a sphere with the same characteristic length as the cylinder). For a spherically symmetric ionic concentration distribution, we can write [14]:

$$\frac{dn(r, t)}{dt} = \frac{D_a}{r^2}\frac{\partial}{\partial r}\left[r^2\frac{\partial r}{\partial n(r, t)}\right] \tag{27}$$

that can be solved (with regard to the boundary condition that ion intensity should vanish at the walls) to yield:

$$n(r, t) = c_2 \exp(D_a c_1 t) \sin(\sqrt{-c_1}\, r)/r \tag{28}$$

where c_1 and c_2 are constants (determined by the boundary conditions) and we take here only the lowest (fundamental) solution of the equation (noting that periodic solutions in multiples of π correspond to higher modes of diffusion that decay more rapidly than the fundamental mode and can for the most part be ignored). Because this equation describes most regions of ionic diffusion, it is extremely informative to show the solution of this equation in Fig. 2. The solution of this equation is the ion density maximum

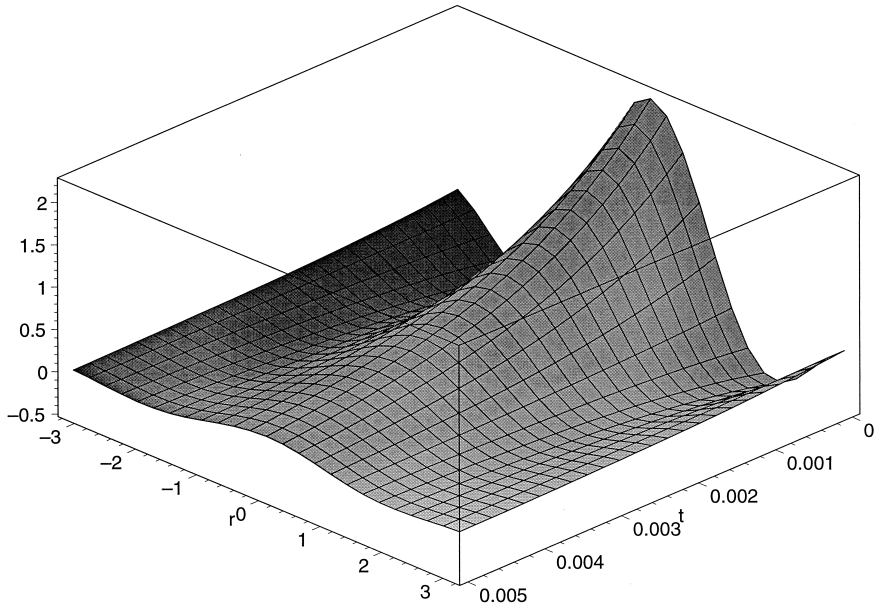

Fig. 2. Representative solution of diffusion Eq. (28) for typical HPMS experiment. Clearly shown is the exponential ion density decay with time and the ionic distribution from the center ($r = 0$) as well as the start of higher diffusion modes.

of the center node representing the center of the spherically symmetric ionic distribution. The ionic intensity is seen to decay exponentially with time (t) (becoming a flatter sine curve) and in addition the approach to higher modes of diffusion are shown. It can be shown that the ambipolar diffusion coefficients D_a and time allowed for diffusion have the same effect on this plot although appropriate boundary conditions would provide quantitative values for the various profiles. Fig. 2 thus depicts the qualitative shape for all time-dependent ionic distributions to be discussed in following sections.

It is of current interest to examine the nature of detected species, thus the nature of the wall current. In stationary afterglow experiments, it is normally assumed that the wall current is driven by the space charge field generated by the large difference in electron and cation mobilities, and thus potential mass discrimination can only occur due to differences in the ambipolar diffusion coefficients *if* the process is diffusion controlled. A small mass discrimination is possible in this region due to differences in ambipolar diffusion coefficients, however, it is not customary to perform equilibria measurements in this region because of the presence of the space charge field. Unknown ambipolar diffusion coefficients can be reliably approximated to $2D^+$, as given by Eq. (18), and subsequently free diffusion coefficients for ions in an excess of neutral gas (as is the case for HPMS experiments) can be approximated theoretically to the classical result from Chapman and Enskog [15]:

$$D = \frac{3}{8n_g Q_d}\left[\frac{\pi kT(m + m_g)}{2mm_g}\right]^{1/2} \tag{29}$$

where n_g is the concentration of neutral, m and m_g are masses of ionic and neutral components, and Q_d is the momentum transfer cross section assumed here to be constant [15]. Because the momentum transfer cross section will be similar for similar ions in the same neutral gas, the ratio of two ambipolar diffusion coefficients can be written

$$\frac{D_{1a}}{D_{2a}} \approx \frac{D_1^+}{D_2^+} = \left[\frac{m_2(m_1 + m_g)}{m_1(m_2 + m_g)}\right]^{1/2} \tag{30}$$

If it is assumed that the wall current is the ionic flux resulting from the diffusion process, then the mass discrimination is small and ordinarily less than any normal experimental uncertainties. For example, experiments involving the first hydration step of Li^+ would have a maximum ratio [Eq. (30)] of about 0.7 leading to a difference in Gibbs energy of about 0.2 kcal mol^{-1} although at masses higher than 30, this effect would be less than 0.93 (in the ratio of diffusion coefficients where a ratio of 1 would be indicative of no mass discrimination) in terms of hydration reactions. These differences in mass represent a small change in the evaluated standard Gibbs energy of reaction and can be ignored here because it is not customary to carry out measurements in the presence of such a large space charge field because of other potential problems. Naturally, a priori knowledge of the ionic mobilities would alleviate the need for any corrections because knowledge of rates of diffusing species would then be known.

2.3. Region II: Cation–anion ambipolar diffusion

The elevated diffusion of ionic species because of cation–electron ambipolar diffusion in early stages of stationary afterglow experiments eventually leads to a breakdown in the space charge field when the number density of electrons decreases below a critical value. At this point (shown schematically in Fig. 1) there is an accompanied slope change in plots of ln n versus t curves corresponding to the boundary between these two processes [16]. In this region the ionic intensities of two ionic species can be written

$$\frac{\partial n_1(r, t)}{\partial t} = -D_{1i}\nabla^2 n_1(r, t) \tag{31}$$

$$\frac{\partial n_2(r, t)}{\partial t} = -D_{2i}\nabla^2 n_2(r, t) \tag{32}$$

where D_{1i} and D_{2i} refer to the cation–anion ambipolar diffusion coefficients given analogously to the electron–ion coefficients by [12]:

$$D_{ni} = 2\,\frac{D^+D^-}{D^+ + D^-} \tag{33}$$

As such any mass discrimination that may occur here would be a function of the ratio of D_{1i}/D_{2i} where it should also be noted that D_{1i} and D_{2i} have values intermediate between the free diffusion coefficients D^+ and D^-.

To analyse the "worst-case" scenario, we assume that the mass of the anionic species is located somewhere between the two cationic species. As an example considering the hydration of a low mass ion such as Li^+, the maximum mass discrimination would be a function of the ambipolar diffusion coefficient ratio of approximately 0.83, corresponding to a difference in free energy of approximately 0.1 kcal mol^{-1}. Equilibria involving higher mass ions would have a significantly smaller mass effect (for example, for hydration of an ion of mass 30 the ratio of ambipolar diffusion coefficients would be less than 1.04, corresponding to a difference of less than 0.02 kcal mol^{-1} that would tend to 0 at higher masses). As such, in the cation–anion ambipolar diffusion region, the potential mass discrimination due to differences in free-diffusion coefficients of the ions can be ignored [3].

2.4. Region III: Free diffusion

Eventually, as in the case of electron–cation ambipolar diffusion, the concentration of anions and hence the overall ionic concentration falls below the critical level (temperature dependent) to maintain cation–anion ambipolar diffusion. Virtually indistinguishable from anion–cation diffusion would be the resultant free diffusion process:

$$\frac{\partial n_1(r, t)}{\partial t} = -D_1^+\nabla^2 n_1(r, t) \tag{34}$$

$$\frac{\partial n_2(r, t)}{\partial t} = -D_2^+\nabla^2 n_2(r, t) \tag{35}$$

where D_1^+ and D_2^+ are the *free*-diffusion coefficients of cations 1 and 2. It can be clearly seen that any potential mass discrimination in an experiment controlled by free diffusion would be given by the ratio D_1^+/D_2^+, the same mass discrimination as illustrated for the case of cation–electron ambipolar diffusion. Examination of the shape of ln n versus t plots would

indicate that the slope between Region II (given by the cation–anion ambipolar diffusion coefficient) and Region III (given by the free-diffusion coefficient) would be virtually indistinguishable. This corresponds to a ratio of slopes of D_{1i}/D_1^+ that can be estimated to be less than <1.2 for very low mass ions, and <1.02 for ions of mass above 30. As such this 2% change in slope is unlikely to be discernible considering the low ion abundances in the free diffusion region. Clearly, all of these regions can be accentuated for reactions involving large mass differences between reactant and product ions. Again, it can be seen here, especially for higher masses, that any effect due to mass discrimination would be significantly less than normal experimental uncertainties.

3. Detected ions

It is clear from the above description that the ion flux is produced by the small concentration gradient present in any reaction chamber and is dependent on the magnitude of the ionic mobilities. However, superimposed on this relatively slow diffusional motion is the thermal motion of the various ions and gases. A typical HPMS or stationary afterglow experiment incorporates a small sampling orifice normally designed to promote molecular flow through the ion exit slit. For example, typical ion exit slit widths of 10 μm [3] and typical operating pressures of 3 mbar would normally lead to molecular flow through the slit. Under these conditions the mean free path of a common bath gas, methane, would be 18 μm. If an ionic species such as Na^+ behaved as a perfect gas particle, its mean free path in methane would be 24 μm, where the contribution due to ion density would be negligible [17]. The mean free paths of ions in the presence of a polarizable neutral are altered due to the mutual potential energy $-(\kappa - 1)e^2/8\pi Nr^4$ between the pair, where κ is the dielectric constant of the gas, e the charge of the ion, and N the number density. As such, the mean free paths of the ions may be reduced by a factor of 3 or more [18] dependent naturally on the polarizability of the neutral molecule. It is likely that for certain common HPMS experimental conditions outlined above ($p \leq 3$ mbar), employing ion exit slits of 10 μm or less, the flow can indeed be classified as molecular. The situation for molecular flow becomes even more favourable at higher temperatures. Various HPMS experiments have employed slightly larger slits or orifices in the attempt to improve ion signal levels. The discussion that follows pertains only to those cases where molecular flow characterizes the ion exit conditions.

The average thermal velocity of ions (assuming a Maxwellian distribution) is given by Eq. (9).

$$\bar{v} = \left(\frac{8kT}{\pi m}\right)^{1/2} \tag{9}$$

The displacement $|\bar{x}|$ of a cloud of ions through a gas by diffusion is given by the Einstein relation [19]:

$$|\bar{x}| = \left(\frac{4Dt}{\pi}\right)^{1/2} \tag{36}$$

This leads directly to the average velocity as a function of time t:

$$\bar{v} = \left(\frac{D}{\pi t}\right)^{1/2} \tag{37}$$

Substitution of appropriate values into Eq. (9) (thermal) and 37 (diffusional) shows immediately that the thermal velocity of the ions far exceeds the average velocity due to diffusion. The average lifetime of a diffusion ion can be written:

$$\tau = \frac{1}{D}\left(\frac{r}{\pi}\right)^2 \tag{38}$$

where τ is the lifetime of the ionic species (time required to reach the wall/slit) and r is the relevant container dimension or distance to the wall/slit. The diffusion velocity at the slit can be simply calculated by:

$$\bar{v}_{slit} = \sqrt{\pi}\,\frac{D}{r} \tag{39}$$

A typical diffusion coefficient, for example NO^+ (in 1 Torr NO), has a coefficient of 42 cm^2/s [12] that leads to a diffusional velocity at the slit of $\bar{v}_{slit} = 149$

cm/s. However, the thermal velocity of NO^+ under these same conditions is approximately 300 times larger than the diffusional velocity.

3.1. Particle exit: Near slit behaviour

In a system of equilibrated particles of differing masses, the Maxwell velocity distribution yields [10]:

$$N_{mf} = \frac{pA}{(2\pi mkT)^{1/2}} \tag{40}$$

where N_{mf} is the number of particles of mass m leaving a slit of area A at a pressure p under molecular flow conditions per unit time. In the absence of any electric fields, the subsequent detected ion abundance is mass dependent:

$$I_x = c_1 \frac{p_x A}{(m_x kT)^{1/2}} \tag{41}$$

where c_1 is some system dependent constant. As such, it is clear that in the absence of any other processes, ions with lighter masses will be sampled more often than those of higher masses in the ratio: $(m_{high}/m_{low})^{1/2}$ directly related to the equation derived by Graham [9]. For this case of molecular flow, a well-characterized mass discrimination results. For the case of a well-defined continuum flow, no mass discrimination would take place [4,5,20], although this often is not an advantageous experimental condition. For certain HPMS experiments, especially those involving clustering equilibria, it is possible that collisions between ionic and other species in the region close to the slit and outside of the ion source may alter the equilibrium distribution of ionic species for continuum flow through the slit. It is also clear that effects of adiabatic cooling become nonnegligible for high flow regimes [3].

It should be noted that although mass discrimination may occur via the diffusion process itself, this will be associated by a change in the slope of ln n versus t plots. However, mass discrimination of the type created by the near-slit thermal motion of the ions will lead only to different absolute values (consistent with time) of the detected individual ion abundances so long as depletion of the source concentrations is controlled more by diffusion to the wall than out of the slit.

3.2. Calculations and experimental comparisons

The equilibrium constant of a typical HPMS experiment was given by Eq. (4):

$$K_{eq} = \frac{I_{B_2H^+} \cdot p_{B_1}}{I_{B_1H^+} \cdot p_{B_2}} \tag{4}$$

However, according to Eq. (41), the actual ion intensities need to be weighted by the square root of mass. As such, we can define the corrected equilibrium constant K_{eq}^{corr} in terms of these corrected ion intensities:

$$K_{eq}^{corr} = \frac{I_{B_2H^+} \cdot p_{B_1}}{I_{B_1H^+} \cdot p_{B_2}} \times \left(\frac{m_{B_2H^+}}{m_{B_1H^+}}\right)^{1/2} \tag{42}$$

It is clear that the described mass discrimination would affect the calculated standard free energy and entropy changes of a reaction, but not the enthalpy change. Using Eq. (42) as a guide, corrected equilibrium constants, standard free energies, and entropies are given (for a reaction Ion1 + neutral1 = Ion2 + Neutral2) by:

$$K_{eq}^{corr} = K_{obs}\left(\frac{m_2}{m_1}\right)^{1/2} \tag{43}$$

$$\Delta G_{eq}^{\circ,corr} = \Delta G_{obs}^{\circ} - \frac{RT}{2} \ln \frac{m_2}{m_1} \tag{44}$$

$$\Delta S_{eq}^{\circ,corr} = \Delta S_{obs}^{\circ} + \frac{R}{2} \ln \frac{m_2}{m_1} \tag{45}$$

where experimentally determined quantities are listed as "obs" and the true or corrected quantities as "eq, corr." As an example for the hydration of Li^+, $m_1 = 7$, $m_2 = 25$, the correction to ΔG_{eq}° would be 0.8 kcal mol^{-1} at 600 K, significantly larger than the normal stated HPMS uncertainty of ± 0.2–0.5 kcal mol^{-1}.

Kebarle and Hogg [21] have measured the conduc-

tances of their ion source exit orifice for He, air, and Xe and noted that the ratio of conductances was inversely proportional to the ratio of the square roots of the molecular weight. They concluded that observed ionic abundances depend on mass, although this correction was not routinely reported in subsequent studies. As discussed earlier, Grimsrud and co-workers have considered the effects of mass discrimination of the neutral components [4,5]. The present results suggest that not only neutral but also ionic mass discrimination be considered. For those reactions involving the measurement of ion abundances for ions of widely different mass, such as results from measurement of clustering and other exchange equilibria, this mass discrimination makes a significant contribution to measured abundances. For reactions involving higher mass ions, the effect is reduced and for mass discrimination effects are often smaller than experimental errors. This is the case for equilibrium reactions involving highly solvated ion clusters where the mass difference between reactant and product ions is small. However, for a large number of reactions this effect should be considered.

We have compared calculated standard free energy changes of reactions from HPMS measurements and those obtained using ion cyclotron resonance[1] equilibria results. Because the majority of HPMS measurements have been obtained at elevated temperatures and ICR measurements mostly near ambient, comparison of results from the two methods is not normally direct. Ideally, comparisons for reaction equilibria measured by both techniques under identical conditions would yield the most meaningful results. However, this was not possible and most often elevated temperature data from HPMS were compared to ICR measurements using the appropriate change in standard entropy (from the same experimental investigation). The elevated temperatures of the HPMS experiments assist in making conditions closer to true molecular flow. We have compared the free energy changes for several common reactions that appear in both HPMS and ICR thermochemical ladders [22–24]. We have limited these comparisons to ratios of m_1/m_2 equal to or greater than 2. The majority of comparisons were based on indirect calculations involving the use of thermodynamic cycles. This may have a slight advantage in that the free energy changes might be more reliable because they are averaged over 2–3 thermodynamic cycles, although there are also associated additive experimental uncertainties. The results of these comparisons are presented in Table 1. There are 18 independent reactions and 27 comparisons in total available in Table 1 to compare HPMS and ICR results, with limited duplicated HPMS data for certain reactions. Of the 27 reactions considered, the mass correction improved the agreement in 21 cases; 6 corrections made the agreement worse. For values in very poor agreement, the correction generally made the discrepancies smaller. In cases where the correction made the spread worse, the corrected values agree in all but one case to the combined experimental uncertainty of the two data sets. It should be noted that using the ICR data from [24] at the originally stated temperature improves these comparisons. Fig. 3 shows the improvement of the HPMS free energies from Szulejko and McMahon [22] and Meot-Ner and Sieck [25] compared with the ICR ladder [23,24] from Table 1. It should be noted that the HPMS measurements of Szulejko and McMahon [22] may not have had strictly molecular flow conditions because of the slightly larger ion exit orifices used, but a flow intermediate between molecular and continuum. This was also the case for Meot-Ner and Sieck [25] who used 60 μm orifices. However, under most conditions, especially those at elevated temperatures, the flow can be stated to be predominantly molecular where these corrections should improve agreement between HPMS and ICR measurements.

[1] We have chosen to compare HPMS results with ion cyclotron resonance because of the reduced mass discrimination possibilities in ICR. Typical pressures in ICR measurements ($\approx 10^{-5}$ mbar) prevent the achievement of equilibrium during normal ion trapping times ($\approx$1 s) for three-body association reactions but these conditions are appropriate for equilibrium transfer reactions. Both types of reactions are amenable to HPMS but we are restricted to comparing only those reactions derived from both methods. Most ICR experiments involve essentially in situ ion detection thereby removing any mass discriminatory effects of having ions pass from the source through a small ion exit slit.

Table 1
Thermochemical data comparison for proton transfer reactions

Reaction	ΔG°_{HPMS}	$\Delta G^{\circ,corr,\ a}_{HPMS}$	$\Delta G^{\circ}_{ICR}{}^{b}$	$\left\lvert\frac{\delta\Delta G^\circ_{corr}}{\delta\Delta G^\circ_{orig}}\right\rvert^{c}$	HPMS ref.
$CF_3CH_2NH_3^+ + NH_3 = NH_4^+ + CF_3CH_2NH_2$	−2.13	−1.59	−1.92	1.57	[25]
$C_6H_5CHCH_3^+ + NH_3 = NH_4^+ + C_6H_5CHCH_2$	−2.88	−2.32	−2.35	0.05	[25]
$CH_3CO_2C_2H_6^+ + NH_3 = NH_4^+ + CH_3CO_2C_2H_5$	−3.69	−3.18	−3.63	7.28	[22]
	−4.26	−3.76	−3.63	0.20	[25]
$(CH_3)_2SH^+ + NH_3 = NH_4^+ + (CH_3)_2S$	−4.29	−3.89	−3.73	0.28	[25]
$(C_2H_5)_2OH^+ + NH_3 = NH_4^+ + (C_2H_5)_2O$	−3.76	−3.31	−3.95	3.43	[22]
$CH_3CO_2CH_4^+ + NH_3 = NH_4^+ + CH_3CO_2CH_3$	−6.78	−6.33	−6.51	0.66	[22]
	−8.74	−8.28	−6.51	0.80	[25]
$(CH_3)_2COH^+ + NH_3 = NH_4^+ + (CH_3)_2CO$	−7.57	−7.19	−7.68	4.28	[22]
	−9.69	−9.31	−7.68	0.81	[25]
$i\text{-}C_4H_9^+ + NH_3 = NH_4^+ + i\text{-}C_4H_8$	−9.55	−9.19	−9.17	0.04	[22]
	−10.94	−10.57	−9.17	0.79	[25]
$i\text{-}C_3H_7CNH^+ + NH_3 = NH_4^+ + i\text{-}C_3H_7CN$	−9.46	−9.03	−9.92	1.93	[22]
	−12.00	−11.56	−9.92	0.79	[25]
$(CH_3)_2OH^+ + NH_3 = NH_4^+ + (CH_3)_2O$	−12.08	−11.77	−11.73	0.12	[22]
	−14.05	−13.74	−11.73	0.87	[25]
$C_2H_5CNH^+ + NH_3 = NH_4^+ + C_2H_5CN$	−14.24	−13.88	−12.05	0.84	[25]
$C_6H_5CH_4^+ + NH_3 = NH_4^+ + C_6H_5CH_3$	−14.27	−13.75	−13.65	0.16	[22]
	−16.57	−16.05	−13.65	0.82	[25]
$CH_2CHCNH^+ + NH_3 = NH_4^+ + CH_2CHCN$	−17.61	−17.26	−14.51	0.89	[25]
$CH_3HCO_2H^+ + NH_3 = NH_4^+ + CH_3HCO_2$	−14.44	−14.05	−14.72	2.37	[22]
	−17.02	−16.63	−14.72	0.83	[25]
$CH_3CNH^+ + NH_3 = NH_4^+ + CH_3CN$	−18.69	−18.42	−15.47	0.92	[25]
$CH_3SH_2^+ + NH_3 = NH_4^+ + CH_3SH$	−20.21	−19.89	−16.64	0.91	[25]
$CH_3CHOH^+ + NH_3 = NH_4^+ + CH_3CHO$	−21.06	−20.77	−17.60	0.92	[25]
$C_6H_7^+ + NH_3 = NH_4^+ + C_6H_6$	−20.55	−20.08	−20.27	0.64	[22]
	−24.23	−23.76	−20.27	0.88	[25]

All the values are in kcal mol^{-1} at 320 K.

[a] HPMS data corrected for mass discrimination.

[b] All ICR data are from [24] and recalculated for 320 K.

[c] The absolute value of the ratio of the difference between corrected HPMS and experimental ICR data and the difference between experimental HPMS and ICR data. Values smaller than 1 indicate improved agreement between HPMS and ICR data after the correction has been applied.

We have also compared results from HPMS and ICR experiments for association reactions as listed in Keesee and Castleman's compilation [26]. Comparisons of these results are presented in Table 2 where all HPMS results stem from direct measurements. Results for ICR experiments were obtained from ICR data for a specific transfer equilibria involving a reference compound combined with HPMS data for the formation of the reference. As an example, Cl^- transfer to benzene is easily measured by HPMS:

$$Cl^- + C_6H_6 = Cl(C_6H_6)^- \quad (46)$$

whereas ICR results were derived from a cycle involving:

$$Cl(C_6H_6)^- + t - BuOH = Cl(t - BuOH)^- + C_6H_6 \quad (47)$$

and auxiliary equilibrium information for

$$Cl(t - BuOH)^- = Cl^- + t - BuOH \quad (48)$$

from HPMS experiments. Combining reactions (47) and (48) leads to the desired reaction given by Eq. (46). In this case, both HPMS and the ICR-cycle data had to be corrected for mass discrimination because the ICR cycle contained results from an HPMS experiment. Reactions whose corrections for both HPMS and ICR were identical were not considered.

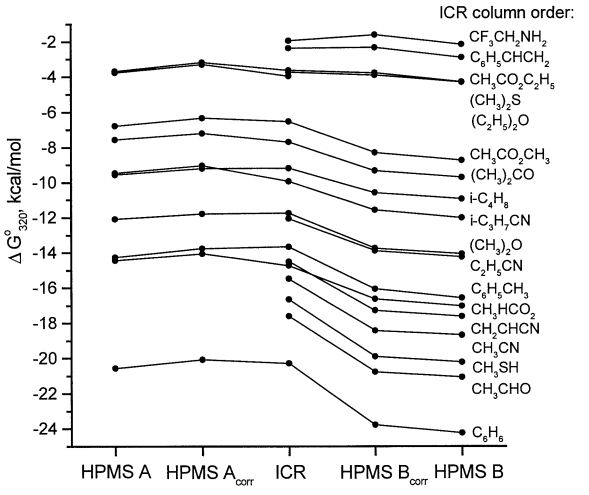

Fig. 3. Thermochemical ladder comparison for proton transfer reactions at 320 K relative to ammonia. The data are taken from Table 1. HPMS "A" data are from [22], HPMS "B" data are from [25], and ICR data are from [24] recalculated at 320 K [23].

The agreement between ICR and HPMS improved for 66% of the reactions considered after applying the appropriate mass corrections. These improvements were small and did not affect the average agreement as observed for the reactions listed in Table 1 because of a few widely disparaging values obtained by HPMS and ICR and because of the various cumulative experimental uncertainties in making these calculations.

From the classical theoretical discussion provided earlier and supported by comparisons provided in Table 1, it is suggested that the correction due to mass discrimination during ion sampling in HPMS or other similar experiments when a ratio of ion abundances are required be applied. Even though experimental uncertainties are often larger than this correction, it is not normally insignificant except for the special case of identical or near-identical mass ions (charge transfer reactions). In some cases it might also be appropriate to include corrections due to differences in ionic mobility, but these corrections (as discussed above) are smaller than those due to sampling and for the most part can be ignored (especially at higher mass). Because of the tendency for further mass discrimination related to the ionic flux to the slit, it is suggested that this well-characterized discrimination be considered.

It is desirable to make a comparative study of specific reactions under identical conditions with large mass ratios of reactant and product ions by HPMS and ICR or similar methods. Such experiments with our newly constructed high-pressure mass spectrometer equipped with a highly stable and known ion source temperature are planned once we can also attempt similar experiments using ICR or some other nondiscriminatory technique.

4. Conclusions

We have examined and characterized the time-dependent ionic profiles that occur in traditional high-pressure mass spectrometric and stationary afterglow experiments. It has been shown that the nature of ionic flow out of an ion source leads to mass discrimination effects related directly to the average velocities of each individual ionic species during conditions normally present in a HPMS or stationary afterglow experiment. These mass discrimination effects are easily calculated and affect standard free energy and entropy changes, but not the corresponding standard enthalpy changes. It was shown that experimental results corrected for mass discrimination are (on average) in better agreement with results without mass discrimination (for example from ICR). As such, it is believed that results from HPMS measurements should be consistently corrected for mass discrimination dependent on the type of flow present. It also appears less problematic to correct molecular flow results for this mass discrimination than continuum flow results for other problems [3].

Acknowledgements

We are grateful to the Swiss National Science Foundation and the ETH Research Commission for grants supporting this research. This article benefited greatly from two anonymous reviewers and we thank them for their careful assessment of this work.

Table 2
Thermochemical data comparison for association reactions

Reaction	ΔG°_{HPMS} [a]	ΔG°_{HPMS} [b]	$\Delta G^{\circ,corr}_{ICR}$ [c]	ΔG°_{ICR} [d]	$\left\lvert\frac{\delta\Delta G^{\circ}_{corr}}{\delta\Delta G^{\circ}_{orig}}\right\rvert$ [e]	Ref. complex[f]
$Cl^- + C_6H_4F_2 = Cl^-(C_6H_4F_2)$	−7.70	−8.13	−8.14	−7.80	0.07	Cl^--t-BuOH
$Cl^- + C_6H_5Cl = Cl^-(C_6H_5Cl)$	−6.50	−6.93	−7.24	−6.90	0.78	Cl^--t-BuOH
$Cl^- + C_6H_6 = Cl^-(C_6H_6)$	−3.80	−4.15	−5.14	−4.80	0.99	Cl^--t-BuOH
$Cl^- + C_6H_6 = Cl^-(C_6H_6)$	−3.60	−3.95	−5.14	−4.80	0.99	Cl^--t-BuOH
$Cl^- + CH_2Cl_2 = Cl^-(CH_2Cl_2)$	−8.90	−9.26	−9.54	−9.20	0.91	Cl^--t-BuOH
$Cl^- + CH_2O_2 = Cl^-(CH_2O_2)$	−20.10	−20.35	−18.74	−18.40	0.95	Cl^--t-BuOH
$Cl^- + CH_2O_2 = Cl^-(CH_2O_2)$	−25.40	−25.65	−18.74	−18.40	0.99	Cl^--t-BuOH
$Cl^- + CH_3Cl = Cl^-(CH_3Cl)$	−4.10	−4.36	−6.54	−6.20	1.04	Cl^--t-BuOH
$Cl^- + CH_3CN = Cl^-(CH_3CN)$	−8.90	−9.13	−9.74	−9.40	1.21	Cl^--t-BuOH
$Cl^- + CH_3CN = Cl^-(CH_3CN)$	−9.20	−9.43	−9.74	−9.40	1.53	Cl^--t-BuOH
$Cl^- + CHCl_3 = Cl^-(CHCl_3)$	−10.80	−11.24	−11.54	−11.20	0.75	Cl^--t-BuOH
$Cl^- + CHCl_3 = Cl^-(CHCl_3)$	−11.80	−12.24	−11.54	−11.20	1.17	Cl^--t-BuOH
$Cl^- + H_2O = Cl^-(H_2O)$	−8.80	−8.92	−8.74	−8.40	0.47	Cl^--t-BuOH
$Cl^- + H_2O = Cl^-(H_2O)$	−9.00	−9.12	−8.74	−8.40	0.64	Cl^--t-BuOH
$Cl^- + H_2O = Cl^-(H_2O)$	−8.20	−8.32	−8.74	−8.40	2.07	Cl^--t-BuOH
$Cl^- + HAc = Cl^-(HAc)$	−15.80	−16.10	−17.04	−16.70	1.05	Cl^--t-BuOH
$Cl^- + HCl = Cl^-(HCl)$	−16.70	−16.91	−16.34	−16.00	0.82	Cl^--t-BuOH
$Cl^- + MeOH = Cl^-(MeOH)$	−10.20	−10.39	−10.24	−9.90	0.52	Cl^--t-BuOH
$Cl^- + MeOH = Cl^-(MeOH)$	−9.80	−9.99	−9.63	−9.40	0.91	Cl^--CH_3CN
$Cl^- + MeOH = Cl^-(MeOH)$	−10.20	−10.39	−9.63	−9.40	0.95	Cl^--CH_3CN
$Cl^- + MeOH = Cl^-(MeOH)$	−9.80	−9.99	−10.24	−9.90	2.44	Cl^--t-BuOH
$Cl^- + NH_3 = Cl(NH_3)$	−3.60	−3.72	−4.84	−4.50	1.24	Cl^--t-BuOH
$Cl^- + SO_2 = Cl^-(SO_2)$	−14.90	−15.21	−15.04	−14.70	0.86	Cl^--t-BuOH
$Cl^- + C_3H_6O = Cl^-(C_3H_6O)$	−7.90	−8.26	−8.54	−8.20	0.93	Cl^--t-BuOH

All the values are in kcal mol^{-1} at 300 K.

[a] All HPMS data are taken from [26].

[b] HPMS data corrected for mass discrimination.

[c] Indirect ICR data corrected for mass discrimination in used HPMS reference data.

[d] All ICR data are taken from [26]. The data are indirect and are referenced to the scale based on a complex indicated in the last column.

[e] The absolute value of the ratio of the difference between corrected HPMS and ICR data and the difference between experimental HPMS and ICR data. Values smaller than one indicate improved agreement between HPMS and ICR data after the corrections have been applied.

[f] Reference complex relative to which ICR data in (d) was calculated.

References

[1] J.L. Franklin, in Ion-Molecule Reactions, Part I, Kinetics and Dynamics, J.L. Franklin (Ed.), Dowden, Hutchinson & Ross, Stroudsburg, 1978, p. 1.

[2] M.T. Bowers, D.H. Aue, H.M. Webb, R.T. McIver, J. Am. Chem. Soc. 93 (1971) 4314; M.V. Buchanan, M.B. Comisarow, in Fourier Transform Mass Spectrometry, Evolution, Innovation, and Applications, M.V. Bunchanan (Ed.), American Chemical Society, Washington, 1987, p. 1.

[3] P. Kebarle, in Techniques for the Study of Ion-Molecule Reactions, J.M. Farrar, W. Saunders Jr. (Ed.), Wiley, New York, 1988, p. 221.

[4] D.S. McGrew, W.B. Knighton, J.A. Bognar, E.P. Grimsrud, Int. J. Mass Spectrom. Ion Processes 139 (1994) 47.

[5] D.H. Williamson, W.B. Knighton, E.P. Grimsrud, Int. J. Mass Spectrom. Ion Processes 154 (1996) 15.

[6] D.R. Zook, E.P. Grimsrud, J. Phys. Chem. 92 (1988) 6374.

[7] K. Hiraoka, K. Morise, T. Shoda, Int. J. Mass Spectrom. Ion Processes 67 (1985) 11.

[8] H.S.W. Massey, E.H.S. Burhop, H.B. Gilbody, Electronic and Ionic Impact Phenomena, 2nd edn., Vols. I–IV, Oxford, London, p. 1969.

[9] J.F. O'Hanlon, A User's Guide to Vacuum Technology, Wiley, New York, 1989, p. 16.

[10] L.B. Loeb, The Kinetic Theory of Gases, McGraw-Hill, New York, 1934.

[11] E.W. McDaniel, Collision Phenomena in Ionized Gases, Wiley, New York, 1964, p. 489.

[12] W.C. Lineberger, L.J. Puckett, Phys. Rev. 186 (1969) 116.

[13] H.S.W. Massey, Slow Collisions of Heavy Particles, in Electronic and Ionic Impact Phenomena, H.S.W. Massey, E.H.S. Burhop, H.B. Gilbody (Eds.), 2nd edn., Vol. III, Oxford, London, 1971, p. 1951.

[14] H.S.W. Massey, H.B. Gilbody, Recombination and Fast Collisions of Heavy Particles, in Electronic and Ionic Impact Phenomena, H.S.W. Massey, E.H.S. Burhop, H.B. Gilbody (Eds.), 2nd edn., Vol. IV, Oxford, London, 1974, p. 2157.
[15] H.S.W. Massey, Slow Collisions of Heavy Particles, in Electronic and Ionic Impact Phenomena, H.S.W. Massey, E.H.S. Burhop, H.B. Gilbody (Eds.), 2nd edn., Vol. III, Oxford, London, 1971, p. 1302.
[16] L.J. Puckett, M.W. Teague, J. Chem. Phys. 54 (1971) 2564.
[17] S. Dushman, Scientific Foundations of Vacuum Technique, Wiley, New York, 1949, p. 38.
[18] L.B. Loeb, Fundamental Processes of Electrical Discharge in Gases, Wiley, New York, 1939, p. 56.
[19] E.A. Mason, E.W. McDaniel, Transport Properties of Ions in Gases, Wiley, New York, 1988, p. 11.
[20] A.H. Shapiro, The Dynamics and Thermodynamics of Compressible Fluids, The Ronald Press Company, New York, 1953.
[21] P. Kebarle, A.M. Hogg, J. Chem. Phys. 42 (1965) 668.
[22] J.E. Szulejko, T.B. McMahon, J. Am. Chem. Soc. 115 (1993) 7839.
[23] S.G. Lias, J.F. Liebman, R.D. Levin, J. Phys. Chem. Ref. Data 13 (1984) 695.
[24] J.F. Wolf, R.H. Staley, I. Koppel, M. Taagepera, R.T. McIver Jr., J.L. Beauchamp, R.W. Taft, J. Am. Chem. Soc. 99 (1977) 5417.
[25] M. Meot-Ner, W. Sieck, J. Am. Chem. Soc. 113 (1991) 4448.
[26] R.G. Keesee, A.W. Castleman Jr., J. Phys. Chem. Ref. Data 15 (1986) p. 1018–1058.